Kinetic Isotope Effects in the Reactions of D Atoms with CH_4, C_2H_6, and CH_3OH: Quantum Dynamics Calculations†

Boutheïna Kerkeni* and David C. Clary*

Physical and Theoretical Chemistry Laboratory, University of Oxford, South Parks Road, Oxford OX1 3QZ, U.K.

Received: April 8, 2004; In Final Form: July 12, 2004

A practical procedure of calculating quantum rate constants for polyatomic reactions presented previously has been extended in this paper to investigate the kinetic isotope effects (KIEs) for the following reactions: D + CH_4, D + C_2H_6, D + C_2D_6, and D + CH_3OH. The method involves treating the quantum dynamics explicitly for bonds being broken and formed with a potential energy surface obtained from ab initio calculations (MP2 for geometry optimizations and vibrational frequencies, CCSD(T) for points on reduced dimensionality surface). Rate constants are evaluated, and we find the existence of inverse and normal kinetic isotope effects among the listed reactions. Comparison with the available experimental measurements for the D + CH_4 and D + CH_3OH reactions confirms the inverse KIE found in the present calculations.

1. Introduction

There has been significant recent progress in applying theoretical methods to treat kinetics and dynamics of polyatomic reactions.[1] The study of kinetic isotope effects (KIEs) on reaction rate constants is an important topic theoretically and experimentally.[2] Such studies can be used to diagnose transition states and also to examine breakage and formation of bonds. Isotopes can also be used as markers to determine the nature of intermediates in chemical reactions.[3] In the case of reactions involving transfer of light atoms such as hydrogen atoms, an accurate description of the KIE normally relies heavily on the importance of a quantum mechanical tunneling description.

In this work, we have investigated the primary isotope effect in abstraction reactions of methane, ethane, and methanol with D atoms. We employed a quantum-based procedure to construct the ab initio potential energy surfaces and performed time-independent calculation of reaction probabilities and rate constants. This procedure has been presented previously by the authors to study the reaction kinetics of hydrogen with methane, ethane, and the two channels of methanol.[4,5] Here, we extend the method to the study of kinetic isotope effects.

Reactions of H atoms with hydrocarbons are important steps in combustion and pyrolysis.[6,7] Intensive experimental investigations have been devoted to clarify the kinetics of the reactions of hydrogen with methane,[8−12] ethane,[13−20] and methanol.[21−31] Measurements of the D + CH_4 rate constants[8] showed a slight curvature in the Arrhenius plot at low temperatures, and larger values than for the H + CH_4 reaction. In the work of Meagher et al.[23] it is reported that the observed isotopic reaction of D with methanol shows an important inverse KIE in the temperature range 298 K ≤ T ≤ 575 K. Whereas in the experimental work of Hoyermann et al.,[25] the authors found similar values for the rate constants at T = 555 K for H + CH_3OH and D + CH_3OH within the limits of error, the H + CD_3OH and H + CD_3OD reactions showed significantly smaller rate constants than the H + CH_3OH reaction over the temperature range 500−680 K. Calculations of the rate constants have been performed for H + C_2H_6[17] and H + CH_3OH[32,33] reactions using transition state theory with tunneling corrections and quantum calculations.[5] These results have been compared with experimental values.

The main objective of this study is to extend a recently developed quantum procedure to treat kinetic isotope effects accurately and with minimal computational cost. We apply the computational procedure that we have been developing that employs a small number of accurate ab initio calculations with quantum scattering computations.[4,5] Thermal rate constants and kinetic isotope effects for the following reactions are computed and compared to existing results from the literature.

$$H + CH_4 \rightarrow H_2 + CH_3 \quad (1)$$

$$D + CH_4 \rightarrow HD + CH_3 \quad (2)$$

$$H + C_2H_6 \rightarrow H_2 + C_2H_5 \quad (3)$$

$$D + C_2H_6 \rightarrow HD + C_2H_5 \quad (4)$$

$$D + C_2D_6 \rightarrow D_2 + C_2D_5 \quad (5)$$

$$H + CH_3OH \rightarrow H_2 + CH_2OH \quad (6)$$

$$H + CH_3OH \rightarrow H_2 + CH_3O \quad (7)$$

$$D + CH_3OH \rightarrow HD + CH_2OH \quad (8)$$

$$D + CH_3OH \rightarrow HD + CH_3O \quad (9)$$

Our procedure involves using hyperspherical quantum dynamics to treat the bonds being broken and formed in the reactions. The effective potential energy surfaces are obtained by optimizing the geometries using the ab initio MP2(full) method, calculating vibrational frequencies using MP2(full) and computing points on the 2D reduced dimensionality surface using CCSD(T,full). Here, we show that this procedure can be extended to calculate KIEs.

† Part of the "Gert D. Billing Memorial Issue".

* To whom correspondence should be addressed. E-mail for B.K.: Boutheina.Kerkeni@chem.ox.ac.uk. E-mail for D.C.C.: David.Clary@chem.ox.ac.uk.

10.1021/jp048440q CCC: $27.50
Published on Web 09/04/2004

The paper is organized as follows. In section 2, we describe briefly the ab initio calculations of the potential energy surfaces, the interpolating method, and the reduced dimensionality quantum scattering theory for reactions 1−9. In section 3 we present the rate constants and the kinetic isotope ratios, discuss the results for these reactions, and make comparisons with available experimental measurements and calculations. Finally our main conclusions are displayed in section 4.

2. Theory

We used the hyperspherical representation (ρ,δ) to describe the reactive process in a polar coordinate transformation from the Jacobi coordinates R_1 and R_2. The reactions studied are of the form $H_a + H_bYZ \rightarrow H_aH_b + YZ$, where Y is the atom from which H_b is abstracted. The distance joining the H_a and H_b atoms is R_2, and the distance between the center of mass of H_aH_b and the center of mass of YZ is R_1. The polar hyperspherical[34,35] coordinates are obtained from the following transformation:

$$\frac{M_1}{\mu}R_1^{\,2} = [\rho\cos(\delta)]^2, \quad \frac{M_2}{\mu}R_2^{\,2} = [\rho\sin(\delta)]^2 \qquad (10)$$

The mass factors are defined as

$$M_1 = \frac{(m_{H_a} + m_{H_b})(m_Y + m_Z)}{(m_{H_a} + m_{H_b} + m_Y + m_Z)}, \quad M_2 = \frac{(m_{H_a} m_{H_b})}{(m_{H_a} + m_{H_b})}, \quad \mu = (M_1 M_2 M_3)^{1/3} \qquad (11)$$

where M_3 is the reduced mass of the product YZ as defined in ref 4.

The grid points required to map all the domains of a given reaction are the $H_a-H_b = R_2$ and $H_b-Y = R_1'$ distances and correspond respectively to the bonds formed and broken where $R_1 = R_1' + R_2M_2$. A transformation from the (R_1,R_2) grid to the hyperspherical coordinates using eq 10 was performed when studying the different isotopes.

2.1. Ab Initio Potential Energy Surfaces. The potential energy surfaces developed in this work treat explicitly the bonds formed and broken (R_1',R_2) and include the zero-point energy for the other degrees of freedom not participating to the reactive process calculated using MP2(full)[36,37] with the cc-pVTZ basis set. In the Born−Oppenheimer approximation, total energies for the isotopic reactions are the same, and for a given set of grid points, total energies are calculated with the CCSD(T,full)[38,39] method and the cc-pVTZ basis set.[40] Force constants for all other vibrational modes are obtained from one frequency calculation at the MP2(full) level and the same basis set, and the normal mode analysis is repeated, for a different isotope, at minimal computational cost. All the ab initio calculations have been performed with the quantum chemistry code Gaussian 98.[41] The additional (but very minor) computational cost when treating the deuterated systems is the MP2 calculations of frequencies at the geometries already optimized. In practice, the cost can be eliminated by storing the MP2 Hessian matrix. The CCSD(T) calculations do not have to be repeated for each isotope.

2.1.1. $H + CH_4 \rightarrow H_2 + CH_3$. A full description of the quantum chemistry calculations for the $H + CH_4$ reaction is given in ref 4. Reaction $D + CH_4$ is found to have a smaller vibrationally adiabatic barrier and is endothermic; the energetics data are reported in Table 1. The transition state has a C_{3v} symmetry and is reactant-like. The potential energy surface is obtained from 40 grid points.

TABLE 1: Energetics of the Isotopic Reactions of Methane, Ethane, and the Channel 1 of Methanol in kcal/mol[a]

	$\Delta V^{\#}$	$\Delta V_a^{\#}$	ΔE	ΔH (0 K)
$H + CH_4$	15.4	14.2	3.6	0.6
$D + CH_4$	15.4	13.26	3.6	0.24
$H + C_2H_6$	13.54	12.0	4.1	1.5
$D + C_2H_6$	13.54	11.1	4.1	0.6
$D + C_2D_6$	13.54	12.34	4.1	2.1
$H + C_2D_6$	13.54	14.65	4.1	4.35
$H + CH_3OH$	9.85	8.56	−5.48	−7.87
$D + CH_3OH$	9.85	7.72	−5.48	−8.74
$D + CD_3OD$	9.85	8.88	−5.48	−7.34
$H + CD_3OD$	9.85	9.75	−5.48	−6.31

[a] $\Delta V^{\#}$ is the classical barrier height, and $\Delta V_a^{\#}$ is the vibrationally adiabatic barrier height. ΔE is the energy change for the reaction excluding vibrational zero-point energies. These are included in the calculation of ΔH.

2.1.2. $H + C_2H_6 \rightarrow H_2 + C_2H_5$. The four isotopic reactions of ethane are characterized by different thermochemistry and reactivity. All four reactions are found to be endothermic, the lowest barrier reaction ($\Delta V_a^{\#} = 11.1$ kcal/mol) is $D + C_2H_6$, and the highest barrier reaction ($\Delta V_a^{\#} = 14.65$ kcal/mol) is $H + C_2D_6$. The analytical surfaces were obtained from 43 grid points. The transition state has a C_s symmetry, and the reactions are reactant-like in view of the small deformation of the bonds at the transition state in comparison to their values in the isolated fragments.

2.1.3. $H + CH_3OH \rightarrow H_2 + CH_2OH$. This reaction presents two reactive channels, as stated previously. The abstraction from the methyl group is the most important.[5,32,33] It is exothermic and has a lower barrier to reaction ($\Delta V_a^{\#} = 8.56$ kcal/mol) compared to the endothermic second channel where the barrier height is ($\Delta V_a^{\#} = 13.29$ kcal/mol).

Four analytical potential energy surfaces (PESs) have been constructed from an average of 50 grid points for the $H/D + CH_3OH$ reactions. Two PESs were required to model the isotopic reactions through channel 1 (i.e., abstraction of H from the methyl side), and two other PESs were required to study the second channel reactivity (i.e., abstraction of H from the hydroxyl side). The $H + CH_3OH$ and $D + CH_3OH$ reactions through channel 1 are found to be exothermic, and the lowest barrier reaction ($\Delta V_a^{\#} = 7.72$ kcal/mol) corresponds to the $D + CH_3OH$ reaction. In channel 2, the $H + CH_3OH$ reaction is endothermic and the $D + CH_3OH$ reaction is exothermic and has a lower barrier to reaction ($\Delta V_a^{\#} = 12.2$ kcal/mol). The key energetics data are listed in Table 1. The transition state structure shows an almost linear H_a-H_b-Y angle and a reactant-like geometry for both channels.

2.1.4. Analytical Representation of the PESs. So far, after transformation from the (R_1,R_2) grid to the (ρ,δ) grid, the effective energies of the ab initio points were fitted to a functional form we have introduced previously.[4] The parameters that enter the functional were optimized numerically using the Gauss−Newton algorithm[42] designed for nonlinear least-squares problems to obtain the best fit to the ab initio grid points in the (ρ,δ) representation.

The analytical forms of the undeuterated $H + C_2H_6$ and $H + CH_3OH$ reactions have already been presented in a previous paper,[5] and a new functional has been developed for the $H + CH_4$ system, where the barrier on the potential is nearer the ab initio value. The forms of the functionals for the isotopic reactions developed in this work are available upon request from the authors.

2.2 Dynamics. To calculate the cumulative reaction probabilities (CRPs) and thereby the rate constants, we performed

quantum dynamics calculations on the analytical potential energy surfaces obtained above. We used the 2D reduced dimensionality model we have presented in earlier work on the H + CH_4, H + C_2H_6, and H + CH_3OH reactions.[4,5] To avoid a rerun of the scattering details, we only present a brief description, and the reader should consult those papers for more details. The 2D Hamiltonian used in our calculations is given by

$$\hat{H} = -\frac{\hbar^2}{2\mu}\frac{\partial^2}{\partial\rho^2} - \frac{\hbar^2}{2\mu\rho^2}\frac{\partial^2}{\partial\delta^2} + \frac{3\hbar^2}{8\mu\rho^2} + \frac{J(J+1)}{2\mu\rho^2} + V(\rho,\delta) \tag{12}$$

where J is the total angular momentum and $V(\rho,\delta)$ is the effective potential energy surface. The integration procedure is made between ρ_{min} and ρ_{max} over N_γ sectors.

The total rate constant was obtained using the energy and the *KJ*-shifting approximations[46,47] applied at the transition state via $Q^{\#}_{rot}$ and $Q^{\#}_{vib}$ partition functions, respectively. This is to account for the $(3N - 8)$ degrees of freedom not explicitly treated in the calculations. It is given by

$$k(T) = \frac{Q^{\#(3N-8)}(T)}{hQ_{react}(T)\,Q_{H_a}(T)}\int_0^\infty \mathrm{d}\,\mathrm{EP}^{J=0}_{cum}(E)\,\mathrm{e}^{-E/(k_BT)} \tag{13}$$

To assess the quantum tunneling effect, we computed also the rate constant k_{TST} from transition state theory:

$$k_{TST}(T) = \frac{Q^{\#}(T)}{hQ_{react}(T)\,Q_{H_a}(T)}\,k_BT\,\mathrm{e}^{-\Delta V^{\#}_a/(k_BT)} \tag{14}$$

The total partition function, Q_{tot}, of a given molecule can be expressed as a product of partition functions for the translational motion and the internal motion (vibration and rotation). These can be calculated within the framework of the rigid-rotor−harmonic-oscillator approximation:

$$Q_{tot} = Q_{trans}Q_{rot}Q_{vib}Q_{elec}$$

$$Q^M_{vib}(T) = \prod_{i=1}^{M}[1 - \exp^{-\hbar\omega_i/(k_BT)}]^{-1}$$

$$Q_{rot}(T) = \sqrt{\frac{\pi T^3}{\Theta_a\Theta_b\Theta_c}}$$

$$\Theta_i = \frac{\hbar^2}{2I_ik_B} \tag{15}$$

where M is the number of vibrations, Q_{react} is the partition function for the reactant, Q_{H_a} is the translational partition function of H_a, and $Q^{\#}(T)$ is the partition function of the transition state.

$$Q^{\#} = Q^{\#}_{trans}VQ^{\#}_{rot}Q^{\#}_{vib}$$

$$Q_{react} = Q^{react}_{trans}\,Q^{react}_{rot}\,Q^{react(3N-6)}_{vib}$$

$$Q_{H_a} = Q^{H_a}_{trans} \tag{16}$$

where V is the volume.

Numerical parameters used in the quantum dynamics calculations for the model are reported in Table 2.

3. Results and Discussion

3.1. Rate Constants. The frequencies and zero-point-energies for all the stationary species are listed in Tables 3−6. In parts a and b of Figure 1 are plotted the quantum and the transition state rate constants and the experimental values from the rate expressions of refs 8, 50, and 51 for the D + CH_4 reaction and of refs 8, 54, and 55 for the H + CH_4 reaction, respectively. In the case of the D + CH_4 reaction, on the same plot are reported the transition state theory (TST) values of Pu and Truhlar.[48] The rate constants by Lawrence et al.[50] were measured by a gas chromatography technique and are given for a low-temperature range; those values are higher than ours by a factor 8 at 300 K and ∼5.7 at 400 K. The measurements of Klein et al.[51] obtained from mass spectrometry are in good agreement with our quantum calculations. The experimental values of Kurylo et al.[8] were analyzed from electron spin resonance; they are ∼4.7 times smaller at 360 K and ∼2.8 smaller at 720 K than our quantum results. First, we see the importance of tunneling in view of the large difference between the quantum

TABLE 2: Values of the Parameters Used in the Scattering Calculations[a]

	channel 1	channel 2	H/D + C_2H_6/C_2D_6	D + CH_4
N	10	10	10	10
N_δ	130	130	130	130
N_γ	146	146	144	140
ρ_{min}	2.7	2.7	3	3.6
ρ_{max}	26	26	26	26
ρ_a	20	20	20	20
ρ_b	26	26	26	26

[a] Distances are in atomic units.

TABLE 3: Normal Mode Analysis of the Stationary Points and Zero-Point Energies at the MP2(full)/cc-pVTZ Level for the D + CH_4 and H + C_2H_6 Reactions

	frequency (cm^{-1})				ZPE (hartree)
DH	3920(a)				0.008 931
D_2	3202(σ_g)				0.007 294
D···H···CH_3 (TS)	1607i (a_1)	503 (e)	503 (e)	1020 (a_1)	0.042 073
	1119 (e)	1119 (e)	1468 (e)	1468 (e)	
	1529 (a_1)	3146 (a_1)	3296 (e)	3296 (e)	
C_2D_5	217 (a″)	579 (a′)	590 (a″)	869 (a′)	0.046 074
	919 (a′)	992 (a″)	1062 (a′)	1095 (a″)	
	1100 (a′)	1228 (a′)	2182 (a′)	2285 (a′)	
	2312 (a′)	2384 (a″)	2410 (a″)		
C_2D_6	242 (a_u)	603 (a_u)	603 (a_u)	867 (a_g)	0.056 621
	996 (a_g)	996 (a_g)	1084 (a_u)	1096 (a_g)	
	1096 (a_g)	1112 (a_u)	1112 (a_u)	1199 (a_g)	
	2225 (a_u)	2232 (a_g)	2341 (a_g)	2341 (a_g)	
	2354 (a_u)	2354 (a_u)			

TABLE 4: Normal Mode Analysis of the Stationary Points and Zero-Point Energies at the MP2(full)/cc-pVTZ Level for the H + C_2H_6 Reaction

	frequency (cm^{-1})				ZPE (hartree)
D···H···C_2H_5 (TS)	1491i (a′)	207 (a″)	229 (a′)	527 (a″)	0.072 036
	841 (a″)	857 (a′)	1035 (a′)	1103 (a′)	
	1130 (a″)	1137 (a′)	1254 (a″)	1417 (a′)	
	1497 (a′)	1512 (a′)	1527 (a″)	1586 (a′)	
	3064 (a′)	3133 (a′)	3154 (a′)	3193 (a″)	
	3217 (a″)				
D···D···C_2D_5 (TS)	1122i (a′)	159 (a″)	214 (a′)	406 (a″)	0.054 697
	606 (a″)	631 (a′)	808 (a′)	829 (a″)	
	879 (a′)	922 (a′)	995 (a″)	1075 (a′)	
	1097 (a′)	1099 (a″)	1206 (a′)	1514 (a′)	
	2212 (a′)	2290 (a′)	2305 (a′)	2372 (a″)	
	2388 (a″)				
H···D···C_2D_5 (TS)	1124i (a′)	170 (a″)	264 (a′)	446 (a″)	0.056 376
	611 (a″)	649 (a′)	842 (a′)	869 (a″)	
	901 (a′)	929 (a′)	995 (a″)	1075 (a′)	
	1098 (a′)	1099 (a″)	1210 (a′)	2018 (a′)	
	2213 (a′)	2291 (a′)	2305 (a′)	2372 (a″)	
	2388 (a″)				

TABLE 5: Normal Mode Analysis of the Stationary Points and Zero-Point Energies at the MP2(full)/cc-pVTZ Level for the H + CH_3OH Reaction

	frequency (cm^{-1})				ZPE (hartree)
CD_3OD	225 (a)	789 (a)	923 (a)	1018 (a)	0.039 101
	1078(*a*)	1108(*a*)	1119 (a)	1183 (a)	
	2204 (a)	2318 (a)	2360 (a)	2340 (a)	
CD_3O	639 (a)	775 (a)	1027 (a)	1028 (a)	0.028 485
	1060 (a)	1204 (a)	2168 (a)	2281 (a)	
	2322 (a)				
CD_2OD	320 (a)	478 (a)	782 (a)	1056 (a)	0.028 843
	1074 (a)	1279 (a)	2328 (a)	2505 (a)	
	2838 (a)				
D···H···CH_2OH (TS1)	1792i (a)	240 (a)	349 (a)	537 (a)	0.048 871
	1028 (a)	1093 (a)	1171 (a)	1225 (a)	
	1287 (a)	1365 (a)	1398 (a)	1518 (a)	
	3118 (a)	3237 (a)	3886 (a)		
CH_3O···H···D (TS2)	2153i (a)	192 (a)	319 (a)	627 (a)	0.047 956
	928 (a)	1065 (a)	1179 (a)	1191 (a)	
	1457 (a)	1480 (a)	1549 (a)	1721 (a)	
	3065 (a)	3133 (a)	3144 (a)		
D···D···CD_2OD (TS1)	1332i (a)	219 (a)	285 (a)	418 (a)	0.037 553
	792 (a)	833 (a)	918 (a)	934 (a)	
	1038 (a)	1078 (a)	1189 (a)	1281 (a)	
	2260 (a)	2410 (a)	2829 (a)		

TABLE 6: Normal Mode Analysis of the Stationary Points and Zero-Point Energies at the MP2(full)/cc-pVTZ Level for the H + CH_3OH Reaction

	frequency (cm^{-1})				ZPE (hartree)
CD_3O···D···D (TS2)	1579i (a)	151 (a)	305 (a)	476 (a)	0.037 143
	697 (a)	889 (a)	926 (a)	1021 (a)	
	1065 (a)	1093 (a)	1176 (a)	1656 (a)	
	2194 (a)	2320 (a)	2334 (a)		
H···D···CD_2OD (TS1)	1345i (a)	250 (a)	322 (a)	471 (a)	0.038 943
	798 (a)	868 (a)	945 (a)	962 (a)	
	1043 (a)	1079 (a)	1213 (a)	1642 (a)	
	2261 (a)	2410 (a)	2829 (a)		
CD_3O···D···H (TS2)	1581i (a)	166 (a)	382 (a)	533 (a)	0.038 942
	738 (a)	891 (a)	926 (a)	1023 (a)	
	1066 (a)	1093 (a)	1176 (a)	2193 (a)	
	2251 (a)	2320 (a)	2334 (a)		

and the classical rate constants. Second, we notice the good agreement between the present TST calculation and those from ref 48. Some of the rate constants are reported in Table 7. The values published by these authors from TST and CVT/μOMT on the MPW60 PES are also displayed. The barriers used by them are 13.7 kcal/mol for D + CH_4 and 14.8 kcal/mol for H + CH_4.

Rate constants versus inverse temperature are displayed in Figure 2 for D + C_2H_6 and D + C_2D_6 reactions. There is a large difference between the quantum values and results from transition state theory in the case of reaction D + C_2H_6, whereas it is smaller in the case of reaction D + C_2D_6. This shows the important tunneling of the H atom abstraction from C_2H_6; deuterium tunnels less efficiently to form D_2 products. There are no results in the literature on these reactions to our knowledge.

From Figure 3, where we plot the thermal quantum and transition state rate constants, we see an important tunneling effect for the D + CH_3OH reaction. It is, however, less than in the case of the C_2H_6 and CH_4 reactions. Also reported in the same figure are values of some experimental measurements from rate expressions of refs 23 and 25 obtained from electron resonance and mass spectrometry techniques, respectively. The results of Hoyermann et al.[25] agree well with the present quantum calculation in the temperature range 500 K $\leq T \leq$ 680 K. The experimental values of Meagher et al.[23] in the temperature range 298−575 K are larger by a factor of 3.6 at

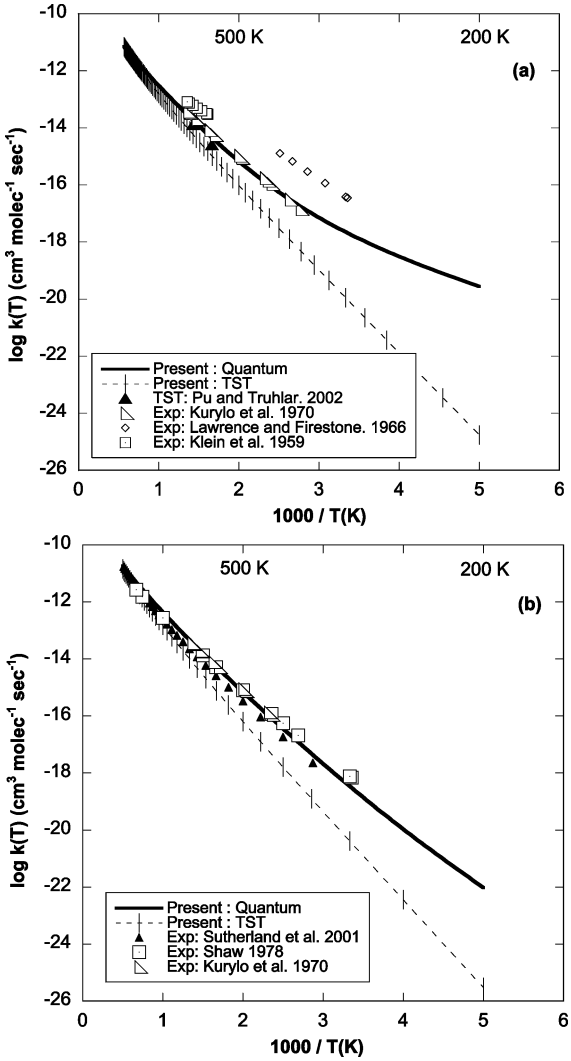

Figure 1. (a) Comparison of the calculated quantum and TST thermal rate constants with results from the literature for D + CH_4 reaction. Experiments are given by the functional form $A\exp(-E/T)$: Kurylo et al.[8] (361−732 K, for $k(T)$, $A = 7.47 \times 10^{-11}$, $E = 5589$); Lawrence et al.[50] (298−398 K, for $k(T)$, $A = 5.99 \times 10^{-11}$, $E = 4279$); Klein et al.[51] (620−738 K, for $k(T)$, $A = 1.65 \times 10^{-11}$, $E = 3920$). Calculated total thermal rate constants are from Table 7. (b) Comparison of the calculated quantum and TST thermal rate constants with results from literature for the H + CH_4 reaction. Experiments are given by the functional form $A\exp(-E/T)$: Sutherland et al.[54] (348−1950 K, for $k(T)$, $A = (6.78 \times 10^{-21})T^{3.156}$, $E = 4406$); Shaw[55] (298−1500 K, for $k(T)$, $A = (2.3 \times 10^{-1})T^{2}$, $E = 4449$); Kurylo et al.[8] (424−732 K, for $k(T)$, $A = 1.04 \times 10^{-10}$, $E = 5837$). Calculated total thermal rate constants are from Table 7.

300 K and 2.5 at 550 K. Some values of the calculated quantum rate constants are reported in Table 8.

3.2. Kinetic Isotope Effects. Kinetic isotope effects are a sensitive test of the potential energy surface and also the properties of the saddle point. In the present work the KIE is defined as the ratio k_i/k_j, where k_i represents the rate constant for the isotopic reaction with heavier mass, and k_j represents the rate constant for the corresponding reaction of H atoms with the undeuterated reactant. With this convention, KIEs greater than 1 are called "inverse" and those less than 1 are called "normal".

The classical calculated KIE from conventional transition state theory and the quantum calculations are reported in Figures 4, 5, and 6 for methane, ethane, and methanol, respectively. We remark that the KIE is larger in the case of the D + CH_4 and

TABLE 7: Comparison between Calculated Thermal and TST Rate Constants with Results from Refs 49 and 48 for the H/D + CH_4 Reactions (in cm^3 $molecule^{-1}$ s^{-1})

T (K)	quantum (R_1)	quantum (R_2)	TST (R_1)	TST (R_1)[49]	TST (R_2)	TST (R_2)[48]	CVT/μOMT (R_2)[48]
200	9.45 (−23)	2.75 (−20)	2.99 (−26)[a]		1.70 (−25)		
250	1.07 (−20)		3.58 (−23)	1.8 (−22)			
300	3.42 (−19)	2.20 (−18)	4.09 (−21)	1.6 (−20)	1.09 (−20)		
400	3.61 (−17)	5.64 (−17)	1.63 (−18)	4.3 (−18)	3.02 (−18)		
600	5.44 (−15)	4.46 (−15)	7.68 (−16)	1.4 (−15)	1.02 (−15)	2.0 (−15)	3.2 (−15)
700	2.48 (−14)	1.87 (−14)	4.78 (−15)	8.0 (−15)	5.83 (−15)	1.1 (−14)	1.4 (−14)
800	7.99 (−14)	5.79 (−14)	1.95 (−14)	3.0 (−14)	2.24 (−14)		
1000	4.37 (−13)	3.04 (−13)	1.5 (−13)	2.1 (−13)	1.6 (−13)		
1500	4.94 (−12)	3.28 (−12)	2.82 (−12)	3.4 (−12)	2.77 (−12)		
2000	1.83 (−11)	1.17 (−11)	1.43 (−11)	3.8 (−11)	1.36 (−11)		

D + C_2H_6 reactions than in the case of the D + CH_3OH reaction. This may be a consequence of quantum tunneling in these reactions, as mentioned in the previous paragraph.

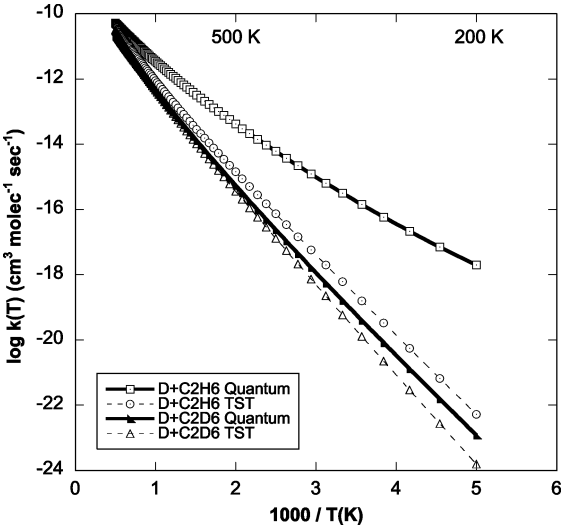

Figure 2. Comparison between the different thermal rate constants from the quantum calculation and the transition state for D + C_2H_6 and D + C_2D_6 reactions.

Because of its smaller vibrationally adiabatic barrier, reaction D + CH_4 shows an inverse kinetic isotope effect at small temperature. At temperatures larger than 500 K, the reaction

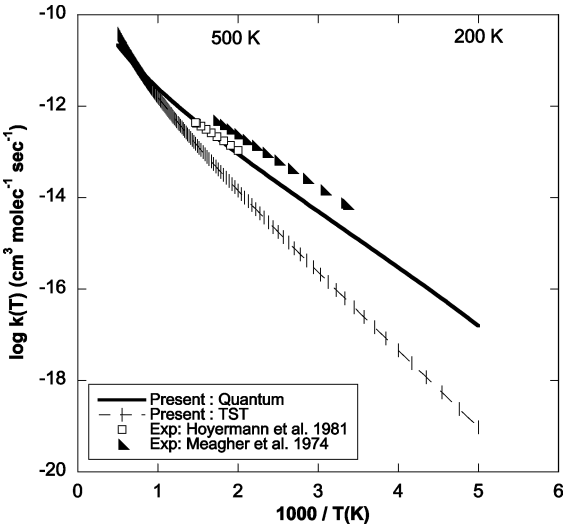

Figure 3. Comparison of the calculated quantum and TST thermal rate constants with results from literature for D + CH_3OH reaction. Experiments are given by the functional form $A\exp(-E/T)$: Hoyermann et al.[25] (500−680 K, for $k(T)$, $A = 2.16 \times 10^{-11}$, $E = 2649$); Meagher et al.[23] (298−575 K, for $k(T)$, $A = 4.68 \times 10^{-11}$, $E = 2619$). Calculated total thermal rate constants are from Table 8.

TABLE 8: Calculated Thermal Rate Constants for the D + C_2H_6/C_2D_6 and D + CH_3OH Reactions (in cm^3 $molecule^{-1}$ s^{-1})

T (K)	D + C_2H_6	D + C_2D_6	D + CH_3OH
200	1.98 (−18)[a]	1.21 (−23)	1.55 (−17)
260	5.83 (−17)	8.18 (−21)	4.59 (−16)
300	3.13 (−16)	1.61 (−19)	1.94 (−15)
360	2.18 (−15)	4.41 (−18)	9.32 (−15)
400	6.04 (−15)	2.39 (−17)	2.07 (−14)
600	1.66 (−13)	4.72 (−15)	2.52 (−13)
700	4.68 (−13)	2.31 (−14)	5.43 (−13)
800	1.06 (−12)	7.81 (−14)	9.90 (−13)
1000	3.51 (−12)	4.55 (−13)	2.41 (−12)
1500	2.01 (−11)	5.46 (−12)	8.93 (−12)
2000	5.18 (−11)	2.07 (−11)	1.90 (−11)

H + CH_4 has the largest rate constant. Some experimental values from ref 8 given by the rate constants $[(6.25 \pm 2.00) \times 10^{13}]\exp[(-11600 \pm 150 \text{ cal mol}^{-1})/(RT)]$ and $[(4.5 \pm 2.00) \times 10^{13}]\exp[(-11100 \pm 150 \text{ cal mol}^{-1})/(RT)]$ cm^3 mol^{-1} s^{-1} for the H + CH_4 and D + CH_4 reactions, respectively, are plotted in Figure 4 and confirm the inverse kinetic isotope effect for this reaction.

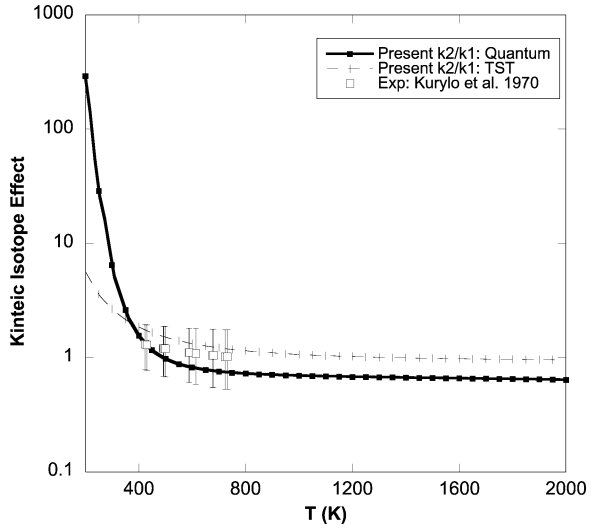

Figure 4. Quantum and classical kinetic isotope effects for the D + CH_4 (k_2/k_1) reaction. In the same figure are plotted experimental values of k_2/k_1 from ref 8.

From the figure we can see that our results are within the error bars of the experiment. We also notice that at temperatures larger than 500 K the KIE becomes normal. This behavior may be associated with the low curvature at these temperatures compared to that at temperatures as low as 200 K. The result from TST shows an inverse KIE for the whole temperature range.

Schatz and co-workers[52] performed conventional transition state theory calculations for many isotopic combinations of the

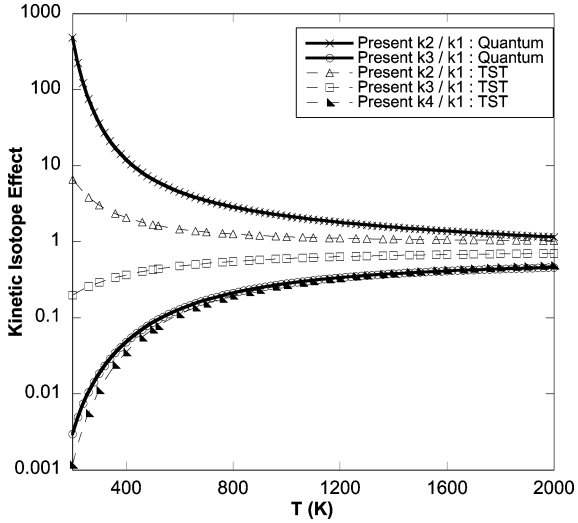

Figure 5. Quantum and classical kinetic isotope effects for D + C_2H_6 (k_2/k_1), D + C_2D_6 (k_3/k_1), and H + C_2D_6 (k_4/k_1) reactions.

TABLE 9: Comparison of the Kinetic Isotope Effects for D + CH_4 Reaction Defined as k_2/k_1 with Available Results

T (K)	present work	Schatz et al.[52]	Pu et al.[48]	Espinosa-García[53]	exptl[8]
400	1.56	1.96	1.81		1.34
500	0.97	1.61	1.56	1.40	1.18
600	0.81	1.42	1.40	1.29	1.08
700	0.75	1.30	1.29	1.21	1.02

H + CH_4 reaction and its reverse. The values the authors found for k_2/k_1 are systematically 30% higher than ours. Truhlar et al.[48] carried out kinetic isotope effects calculations for the isotopic variants of the H + CH_4 reaction in both the forward and reverse directions on different parametrized potential energy surfaces, obtained using variational transition state theory with mutidimensional tunneling (VTST/MT). Espinosa-García[53] also investigated kinetic isotope effects calculations on eight deuterated reactions involving methane. The author developed a new semiempirical potential energy surface for H + CH_4 and performed VTST/MT calculation of the rate constants over the temperature range 300−2000 K. The kinetic isotope effect results from those studies are reported in Table 9 for comparison with the present investigations on the D + CH_4 system.

Reaction D + C_2H_6 shows an inverse kinetic isotope effect for the whole temperature range in the case of TST and quantum calculations respectively (see Figure 5). This behavior is caused by the low vibrationally adiabatic barrier on the PES of reaction 4 and its larger transition state vibrational partition function. However, for reaction 5, the vibrationally adiabatic barrier height is higher than that for reactions 3 and 4, and hence, the KIE is normal because of the very small tunneling found in this reaction as stated previously. We notice that the quantum prediction of the kinetic isotope effects for reaction 5 is smaller than the transition state theory values. This may be assigned to a large barrier width for this reaction. Reaction H + C_2D_6 has the largest barrier height, and for this reason, it presents a normal classical KIE. To our knowledge, there are no experimental investigations on the isotopic reactions of ethane.

Investigations of the D + CH_3OH reaction showed inverse kinetic isotope effects for the whole temperature range. Some experimental values of Meagher et al.[23] given in the range 298 K ≤ T ≤ 575 K by $[(1.80 \pm 0.33) \times 10^{13}]\exp[(-5440 \pm 130$ cal mol^{-1})/(RT)] and $[(2.82 \pm 0.40) \times 10^{13}]\exp[(-5200 \pm 100$ cal mol^{-1})/(RT)] cm^3 mol^{-1} s^{-1} for the H + CH_3OH and D + CH_3OH reactions, respectively, are reported in Figure 6. The

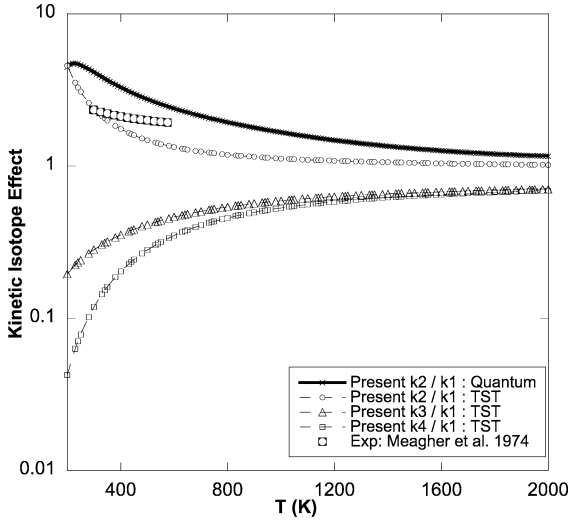

Figure 6. Quantum and classical kinetic isotope effects for reactions D + CH_3OH (k_2/k_1), D + CD_3OD (k_3/k_1), and H + CD_3OD (k_4/k_1). In the same figure are plotted experimental values of k_2/k_1 from refs 23 and 25.

comparison shows an agreement within a factor 2 at 300 K and 1.3 at $T \approx 500$ K with the present quantum calculations. Results from transition state theory show that only the D + CH_3OH reaction that has the lowest barrier height ($\Delta V_a^{\#} = 7.72$ kcal/mol) has an inverse KIE for the whole temperature range when compared to the D + CD_3OD and H + CD_3OD reactions.

4. Conclusions

In this paper we have investigated the effect of quantum tunneling on the reactivity and kinetic isotope effects in abstraction reactions of H + CH_4, H + C_2H_6, and H + CH_3OH. This has been achieved by extending a combined ab initio and quantum dynamics procedure of calculating rate constants to these reactions. We compared the results with the available calculations and experimental values of kinetic isotope effects for the D + CH_4 and D + CH_3OH reactions. The predicted inverse kinetic isotope effects agree with the experiments and previous calculations.

Acknowledgment. This work was supported by the Engineering and Physical Sciences Research Council and the European Union Framework V Programme.

References and Notes

(1) Althorpe, S. C.; Clary, D. C. *Annu. Rev. Phys. Chem.* **2003**, *54*, 493.
(2) Hu, W.-P.; Rossi, I.; Corchado, J. C.; Truhlar, D. G. *J. Phys. Chem. A* **1997**, *101*, 6911.
(3) Zhao, F.; Ghezzo-Schöneich, E.; Aced, G.; Hong, J.; Milby, T.; Schöneich, C. *J. Biol. Chem.* **1997**, *272*, 9019.
(4) Kerkeni, B.; Clary, D. C. *J. Chem. Phys.* **2004**, *120*, 2308.
(5) Kerkeni, B.; Clary, D. C. *J. Chem. Phys.*, in press.
(6) Aronowitz, D.; Naegeli, D. W.; Glassman, I. *J. Phys. Chem.* **1977**, *81*, 2555.
(7) Jones, D.; Morgan, P. A.; Purnell, J. H. *J. Chem. Soc., Faraday. Trans. 1* **1977**, *73*, 1311.
(8) Kurylo, M. J.; Hollinden, G. A.; Timmons, R. B. *J. Chem. Phys.* **1970**, *52*, 1773.
(9) Shaw, R. *J. Phys. Chem. Ref. Data* **1978**, *7*, 1179.
(10) Sepehrad, A.; Marshall, R. M.; Purnell, J. H. *J. Chem. Soc., Faraday Trans. 1* **1979**, *75*, 835.
(11) Baulch, D. L.; Cobos, C. J.; Cox, R. A.; Esser, C.; Frank, P.; Just, Th.; Kerr, J. A.; Pilling, M. J.; Troe, J.; Walker, R. W.; Warnatz, J. *J. Phys. Chem. Ref. Data* **1992**, *21*, 411.
(12) Sutherland, J. W.; Su, M.-C.; Michael, J. V. *Int. J. Chem. Kinet.* **2001**, *33*, 669.

(13) Azatyan, V. V.; Filippov, S. B. *Dokl. Phys. Chem. (Engl. Transl.)* **1969**, *184*, 49.
(14) Lede, J.; Villermaux, J. *Can. J. Chem.* **1978**, *56*, 392.
(15) Reference deleted in proof.
(16) Jones, W. E.; Ma, J. L. *Can. J. Chem.* **1986**, *64*, 2192.
(17) Bryukov, M. G.; Slagle, I. R.; Knyazev, V. D. *J. Phys. Chem. A* **2001**, *105*, 6900.
(18) Baulch, D. L.; Cobos, C. J.; Cox, R. A.; Esser, C.; Frank, P.; Just, Th.; Kerr, J. A.; Pilling, M. J.; Troe, J.; Walker, R. W.; Warnatz, J. *J. Phys. Chem. Ref. Data* **1992**, *21*, 411.
(19) Tsang, W.; Hampson, R. F. *J. Phys. Chem. Ref. Data* **1986**, *15*, 1087.
(20) Camilleri, P.; Marshall, R. M.; Purnell, J. H. *J. Chem. Soc., Faraday Trans. 1* **1974**, *70*, 1434.
(21) Aders, W. K.; Wagner, H. Gg. *Z. Phys. Chem.* **1971**, *74*, 224.
(22) Aders, W. K. *Reactions of H-Atoms with Alcohols*; Weinberg, F., Ed.; Combustion Institute, European Symposium; Academic Press: London 1973; Vol. 1, p 19.
(23) Meagher, J. F.; Kim, P.; Lee, J. H.; Timmons, R. B. *J. Phys. Chem.* **1974**, *78*, 2650.
(24) Westbrook, C. K.; Dryer, F. L. *Combust. Sci. Technol.* **1979**, *20*, 125.
(25) Hoyermann, K.; Sievert, R.; Wagner, H. Gg. *Ber. Bunsen-Ges. Phys. Chem.* **1981**, *85*, 149.
(26) Vandooren, J.; Van Tiggelen, P. J. *Experimental Investigation of Methanol Oxidation in Flames: Mechanisms and Rate Constants of Elementary Steps*; Combustion Institute: Pittsburgh, PA, 1981; Vol. 18, p 473.
(27) Warnatz, J. *Rate Coefficients in the C/H/O System Combustion Chemistry*; Gardiner, W. C., Jr., Ed.; Springer-Verlag: New York 1984; p 197.
(28) Spindler, K.; Wagner, H. Gg. *Ber. Bunsen-Ges. Phys. Chem.* **1982**, *86*, 2.
(29) Cribb, P. H.; Dove, J. E.; Yamazaki, S. *Combust. Flame.* **1992**, *88*, 169.
(30) Li, S. C.; Williams, F. A. *Symp. (Int.) Combust., [Proc.]* **1996**, *26*, 1017.
(31) Dóbé, S.; Bérces, T.; Turányi, T.; Márta, F.; Grussdorf, J.; Temps, F.; Wagner, H. Gg. *J. Phys. Chem.* **1996**, *100*, 19864.
(32) Lendvay, G.; Bérces, T.; Márta, F. *J. Phys. Chem.* **1997**, *101*, 1588.
(33) Jodkowski, J. T.; Rayez, M.-T.; Rayez, J.-C. *J. Phys. Chem.* **1999**, *103*, 3750.
(34) Schmatz, S.; Clary, D. C. *J. Chem. Phys.* **1998**, *109*, 8200.
(35) Pack, R. T. *Chem. Phys. Lett.* **1984**, *108*, 333.
(36) Møller, C.; Plesset, M. S. *Phys. Rev.* **1934**, *46*, 618.
(37) Head-Gordon, M.; Pople, J. A.; Frisch, M. J. *Chem. Phys. Lett.* **1988**, *153*, 503.
(38) Pople, J. A.; Head-Gordon, M.; Raghavachari, K. *J. Chem. Phys.* **1987**, *87*, 5968.
(39) Watts, J. D.; Bartlett, R. J. *Int. J. Quantum Chem.* **1993**, *S27*, 51.
(40) Dunning, T. H. *J. Chem. Phys.* **1989**, *90*, 1007.
(41) Frisch, M. J.; Trucks, G. W.; Schlegel, H. B.; Scuseria, G. E.; Robb, M. A.; Cheeseman, J. R.; Zakrzewski, V. G.; Montgomery, J. A., Jr.; Stratmann, R. E.; Burant, J. C.; Dapprich, S.; Millam, J. M.; Daniels, A. D.; Kudin, K. N.; Strain, M. C.; Farkas, O.; Tomasi, J.; Barone, V.; Cossi, M.; Cammi, R.; Mennucci, B.; Pomelli, C.; Adamo, C.; Clifford, S.; Ochterski, J.; Petersson, G. A.; Ayala, P. Y.; Cui, Q.; Morokuma, K.; Malick, D. K.; Rabuck, A. D.; Raghavachari, K.; Foresman, J. B.; Cioslowski, J.; Ortiz, J. V.; Stefanov, B. B.; Liu, G.; Liashenko, A.; Piskorz, P.; Komaromi, I.; Gomperts, R.; Martin, R. L.; Fox, D. J.; Keith, T.; Al-Laham, M. A.; Peng, C. Y.; Nanayakkara, A.; Gonzalez, C.; Challacombe, M.; Gill, P. M. W.; Johnson, B. G.; Chen, W.; Wong, M. W.; Andres, J. L.; Head-Gordon, M.; Replogle, E. S.; Pople, J. A. *Gaussian 98*, revision A.3; Gaussian, Inc.: Pittsburgh, PA, 1998.
(42) Gill P. E.; Murray, W. *SIAM J. Numer. Anal.* **1978**, *15*, 977.
(43) Muckerman, J. T. *Chem. Phys. Lett.* **1990**, *173*, 200.
(44) Light, J. C.; Walker, R. B. *J. Chem. Phys.* **1976**, *65*, 4272.
(45) Clary, D. C. *Phys. Chem. Chem. Phys.* **1999**, *1*, 1173.
(46) Bowman, J. M. *Adv. Chem. Phys.* **1985**, *61*, 115.
(47) Bowman, J. M. *Reaction and Molecular Dynamics*; Springer: New York, 2000.
(48) Pu, J.; Truhlar, D. G. *J. Chem. Phys.* **2003**, *117*, 10675.
(49) Pu, J.; Truhlar, D. G. *J. Chem. Phys.* **2002**, *116*, 1468.
(50) Lawrence, R. H.; Firestone, R. F. *J. Am. Chem. Soc.* **1966**, *88*, 4564.
(51) Klein, R.; McNesby, J. R.; Scheer, M. D.; Schoen, L. J. *J. Chem. Phys.* **1959**, *30*, 58.
(52) Schatz, G. C.; Wagner, A. F.; Dunning, T. H., Jr. *J. Phys. Chem.* **1984**, *88*, 221.
(53) Espinosa-García, J. *J. Chem. Phys.* **2002**, *116*, 10664.
(54) Sutherland, J. W.; Su, M.-C.; Michael, J. V. *J. Chem. Kinet.* **2001**, *33*, 669.
(55) Shaw, R. *J. Phy. Chem. Ref. Data* **1978**, *7*, 1179.